

In Situ Bottom-up Synthesis of Porphyrin-based Covalent Organic Frameworks

Elham Tavakoli^{a*}, Arvin Kakekhani^{b*}, Shayan Kaviani^{c*}, Peng Tan^{b,d}, Mahdi Mohammadi
Ghaleni^c, Mohsen Asle Zaeem^e, Andrew M. Rappe^b, Siamak Nejati^{a,c}

^a *Department of Mechanical and Materials Engineering,
University of Nebraska-Lincoln, Lincoln, NE 68588-8286, USA*

^b *Department of Chemistry, University of Pennsylvania,
Philadelphia, Pennsylvania 19104-6323, USA*

^c *Department of Chemical and Biomolecular Engineering,
University of Nebraska-Lincoln, Lincoln, NE 68588-8286, USA*

^d *Department of Physics, Harbin Institute of Technology,
Harbin 150001, China*

^e *Department of Mechanical Engineering, Colorado School of Mines,
Golden, CO 80401-1887, USA*

* *Contributed equally*

KEYWORDS: *covalent organic frameworks, porphyrin, Pyridine, Co-crystallization, crystalline dendrite, π - π stacking, oxygen reduction reaction, density functional theory*

ABSTRACT: Synthesis and processing of two- or three-dimensional covalent organic frameworks (COFs) have been limited by solvent intractability and sluggish condensation kinetics. Here, we report on the electrochemical deposition of poly(5,10,15,20-tetrakis (4-aminophenyl) porphyrin)-covalent organic frameworks (POR-COFs) via formation of phenazine linkages. By adjusting the synthetic parameters, we demonstrate the bottom-up synthesis of COF dendrites. Both experiment and density functional theory

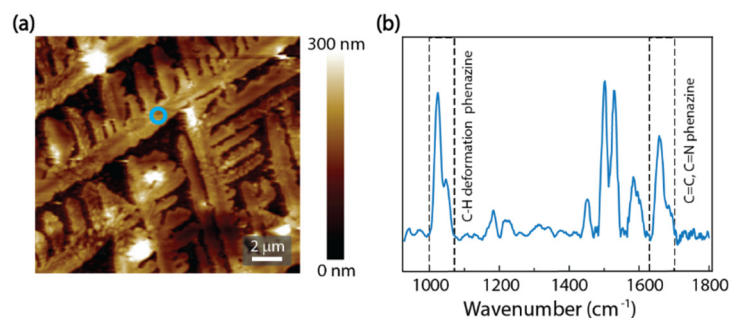
1 (DFT) underline the prominent role of pyridine, not only as a polymerization promoter, but as a stabilizing
2 sublattice, co-crystallizing with the framework. The crucial role of pyridine in dictating the structural
3 properties of such a co-crystal (Py-POR-COF) is discussed. Also, a structure-to-function relationship for
4 this class of materials, governing their electrocatalytic activity for the oxygen reduction reaction (ORR)
5 in alkaline media, is reported.

6 Covalent organic frameworks (COFs) represent organized and intrinsically porous networks constructed
7 using a variety of rigid organic units.¹ Among various building blocks of COFs, macrocyclic structures
8 such as phthalocyanine and porphyrin are of special interest due to their metal coordination chemistry.²⁻⁵
9 Having delocalized π -electrons and high surface area, the porphyrin-based COFs (POR-COFs) have found
10 applications in optoelectronic, molecular electronics, separation, and catalysis.⁶⁻¹⁰ Despite the promises
11 of POR-COFs in electrocatalysis, especially in carbon dioxide and oxygen electroreduction, their
12 processing is hindered by their low solubilities.¹¹⁻¹² The electroreduction of oxygen on porphyrinic
13 structures is of special interest, as the respiratory enzymes with similar active centers catalyze this reaction
14 in-vivo, with an unsurpassed selectivity.¹³ Development of porphyrin-based ORR catalysts has thus been
15 an active research field,^{12, 14-16} achieving electrocatalytic activities comparable to those of Pt-based
16 catalysts.¹⁷⁻¹⁸ Here, we demonstrate a novel approach for assembling POR-COFs via in-situ
17 electrocrystallization of 5,10,15,20-tetrakis(4-aminophenyl)porphyrin known as TAPP. We discuss the
18 importance of stacking the 2D-COF sheets and intercalated guest molecules¹⁹ in determining the structure
19 and subsequently the electrocatalytic activity of such frameworks.

20 We use a three-electrode electrochemical cell connected to a potentiostat for the electrodeposition of
21 TAPP. The electropolymerization is performed through galvanostatic, potentiostatic, and
22 potentiodynamic methods in a solution of TAPP monomer in dichloromethane, containing supporting
23 electrolyte salt and pyridine; a Ag/AgNO₃ electrode and a platinum gauze are used as the reference and
24 counter electrodes, respectively. The polymerization proceeds via formation of radical cations of TAPP,
25 followed by a series of coupling reactions of the oxidized para-aminophenyl substituents. Initially,
26 diphenylamines form, and subsequently they convert to dihydrophenazines and phenazine linkages (see
27 Section 2.3 of the Supporting Information).^{16, 20}

28 Fourier-transform infrared spectroscopy (FTIR), X-ray photoelectron spectroscopy (XPS), and X-ray
29 diffraction (XRD), shown in Figures S2-4, were performed to characterize the electrodeposited materials.
30 As shown in Figure 1a, atomic force microscope infrared spectroscopy (AFM-IR) reveals that the
31 deposited films on the glassy carbon (GC) electrode possess dendritic-like structures and are organic. The
32 deposited films remain stable upon lifting and transfer to a polar aprotic solvent such as acetonitrile (see
33 Figures S5 and S6). The IR spectra of the dendrites (see Figure 1b) agrees with the FTIR spectra of the

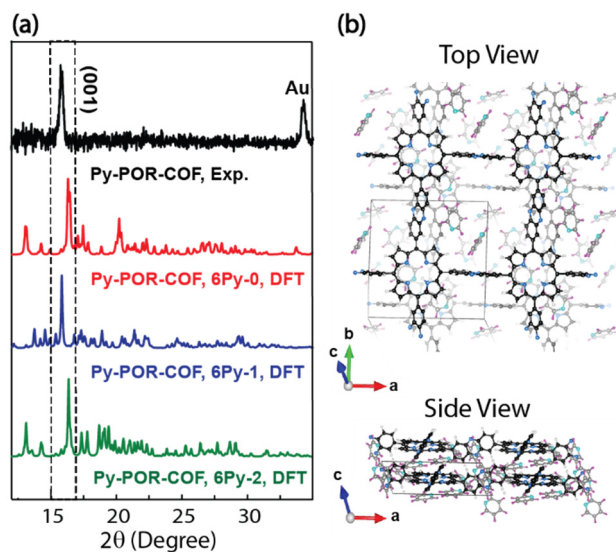
1 free-standing polymeric film of TAPP (pTAPP), synthesized after Walter et al.²⁰ As shown in Figures 1b
2 and S2, the characteristic peaks of pTAPP appeared between 1000-1100 cm⁻¹ and 1660-1630 cm⁻¹. We
3 assigned the former to the C-H deformations of the phenyl rings, beta-pyrrolic, and phenazine ring, and
4 the latter to the C=C and C=N of phenazine ring vibrations.²¹⁻²² XPS reveals that the films are organic,
5 and a small content of fluorine in the samples was assigned to the residual hexafluorophosphate (PF₆⁻)
6 anion (section 3.2 of Supporting Information). The X-ray diffractograms for the pTAPP dendrites,
7 deposited on gold and GC electrodes, are shown in Figures 2a and 4S, respectively. The diffraction
8 patterns demonstrate a distinct peak at 15.8 degrees. This peak is the fingerprint of crystalline pTAPP
9 corresponding to an interlayer distance of 5.60 Å for the stacked 2D-COF sheets. However, such spacing
10 is unexpectedly large for COFs.²³⁻²⁵ Our DFT calculations reveal that the pyridine molecules can
11 intercalate within the pTAPP network and increase the interlayer spacing between the 2D sheets (see
12 Figure 2a). Our calculations suggest that the experimental samples possess a (6:1) ratio of pyridine to
13 TAPP (Figure 2b). Such a structure is polymorphous; for example, for each TAPP molecule, zero, one or
14 two out of the six pyridine molecules (denoted by 6Py-0, 6Py-1 and 6Py-2, respectively), can be located
15 between the stacked porphyrin rings. These configurations are close in energy (within 2 meV per atom)
16 and can be thermally explored. The simulated XRD patterns for a few such structures are shown in Figure
17 2a. A common feature among these patterns is the peak appearing around 15.8 degrees.



18

19 **Figure 1.** (a) AFM height image of pTAPP, electrodeposited on GC electrode. (b) FT-IR spectra of a spot
20 (the blue circle in (a)) on the dendrite. The electropolymerization was carried out in a 5% v/v pyridine in
21 dichloromethane solution containing 0.25 mM TAPP and 0.05 M TEA(PF₆) as the supporting electrolyte
22 salt.

23

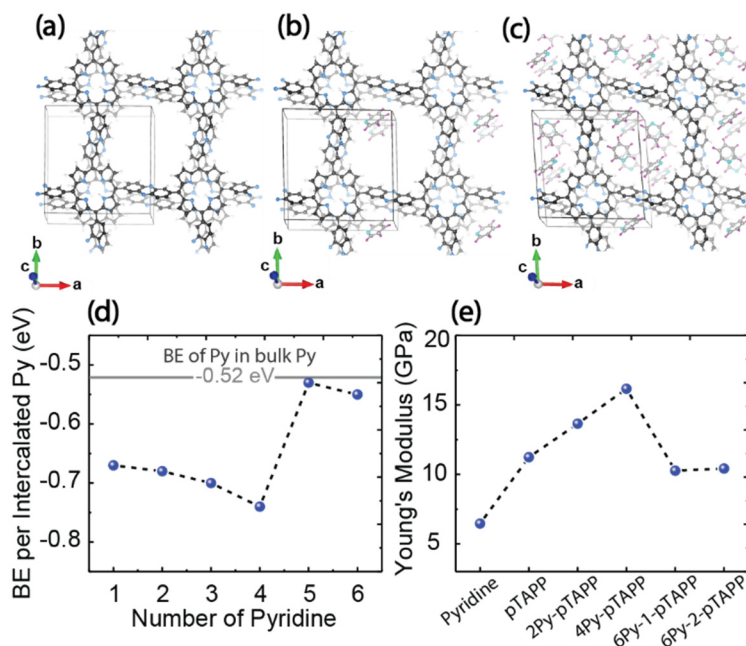


1

2 **Figure 2.** (a) Experimental XRD pattern of Py-POR-COF electropolymerized on a gold substrate, along
 3 with the DFT-predicted XRD patterns for a few heterostructures with 6 pyridines per pTAPP unit. The
 4 electropolymerization of TAPP was carried out in a solution containing 0.25 mM TAPP and 0.05 M
 5 TEA(PF₆) as the supporting electrolyte salt, and 5% v/v pyridine in dichloromethane. (b) The DFT-
 6 derived structure for the lowest internal-energy structure with 6 pyridines (6Py-2). The color code for
 7 COF is: C (black), N (blue) and H (white). For pyridine: C (gray), N (cyan) and H (magenta). The a, b
 8 and c axes are the cell lattice vectors.

9 Here, the non-planar geometry of TAPP (see Figure S16) forces the resulting POR-COF structure into an
 10 inclined (J-aggregate) stacking, allowing accommodation of the maximal π - π stacking between the
 11 layers.^{23,26} Additionally, the pyridine additive not only neutralizes protonated amine groups and increases
 12 the polymerization efficiency,²⁰ but also stabilizes the overall heterostructure and improves the
 13 crystallinity through co-electrocrystallization with the pTAPP. This phenomenon is presented in Figure
 14 3d, where the intercalated pyridine is shown to bring down the internal energy of the whole system. The
 15 structure with four pyridines (per TAPP) is a thermodynamic sink, when the internal energy contribution
 16 alone is considered. Comparing Young's moduli of structures with four and six pyridines (4- and 6-Py),
 17 shown in Figure 3e, we conclude that the latter is considerably softer. This softness and the excess free
 18 volume of the 6-Py structures lead to increased entropy and lower Gibbs free energy for the system.
 19 Therefore, we expect entropy stabilization to play a role in experimental realization of the 6-Py phase (for
 20 more details see Section 4 of the Supporting Information). By examining Figures 3a-c and Figure 2b, we
 21 note that increasing the pyridine content enhances the tilting of the J-aggregate stacking. This
 22 phenomenon is concomitant with an increase in the estimated interlayer distance. Nonetheless, the average
 23 values for the peak position in the simulated XRD, shown in Figure 2a, are slightly higher when compared
 24 with the position of the peak in the experimental result. We attribute this discrepancy to the out-of-plane

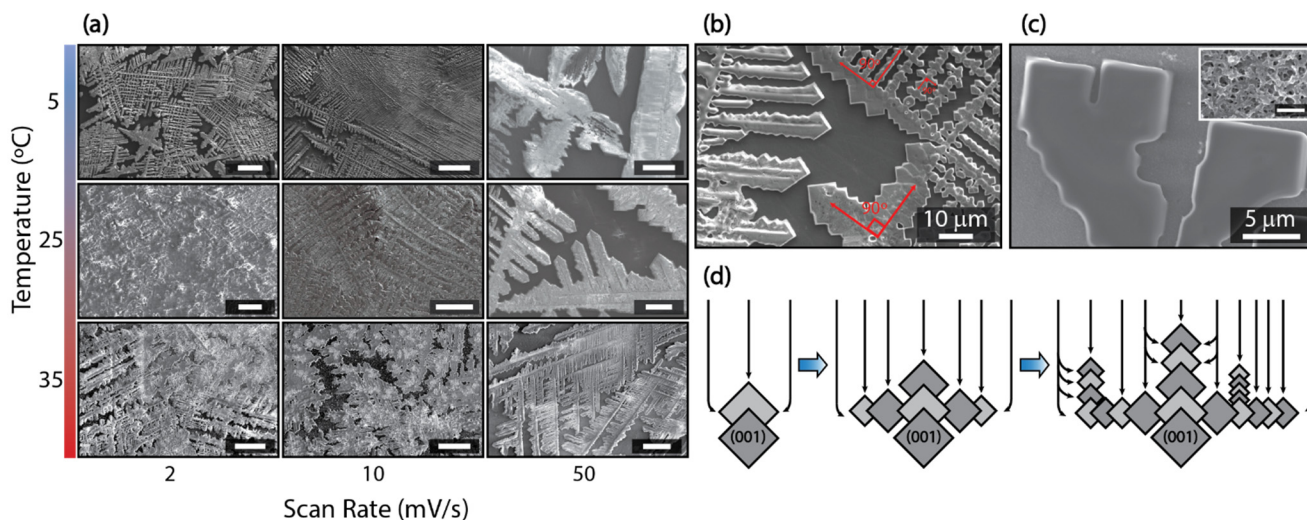
1 thermal expansion of the structure, not accounted for in DFT models. For details on the elastic moduli
2 and other DFT calculations, see Section 4 of the Supporting Information.



3

4 **Figure 3.** The DFT-derived structures for Py-POR-COF with 0 (a), 1 (b) and 4 (c) intercalated pyridines.
5 The color code for the atoms is the same as in the previous figure. (d) Binding energy (BE) of pyridine
6 (Py) in Py-POR-COF computed relative to the bare stacked COF and bulk pyridine phase. (e) Young's
7 modulus for some relevant material phases.

8 In order to understand the parameters influencing the morphology of pTAPP, we performed set of
9 electropolymerization experiments. Figure 4a demonstrates the morphological changes of pTAPP as a
10 function of temperature and potential scanning rate. The statistical analyses on the SEM images (Figure
11 S8) suggest that the dendrite size increases at lower temperatures or higher scan rates. It has been
12 previously proposed that dendrite growth during electropolymerization is governed by the linear and
13 spherical diffusion of the active species to the electrode surface.²⁷⁻²⁹ Here, we assume that the dendrite
14 growth starts with the initial coverage of the substrate by pTAPP nanowire networks.¹⁷ Soon after the
15 dendrite nucleation takes place, due to the spherical diffusion on the nuclei and protrusions (Figure 4d),
16 pTAPP crystals grow from the edges of {110} planes.³⁰ The impact of the diffusion boundary layer on
17 the electropolymerization of TAPP and the formation of dendrites are discussed in Section 3.6 of the
18 Supporting Information. To elucidate the effect of substrate on the electropolymerization of TAPP, we
19 performed experiments on substrates with various surface energies and roughness factors. As shown in
20 Figures S11-15, a smoother surface favors formation of larger dendrites through providing fewer possible
21 nucleation sites; therefore, greater distances may exist around each nucleus, permitting growth of larger
22 dendrites.



1

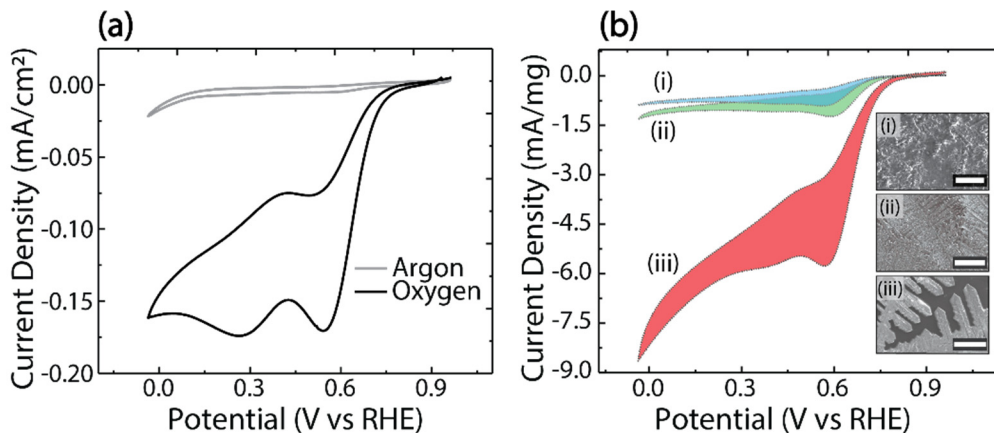
2 **Figure 4.** (a) SEM images of pTAPP films, electrodeposited with scan rates of 2 mV/s, 10 mV/s, and
 3 50 mV/s at temperatures of 5 °C, 25 °C, and 35 °C on GC (scale bar is 50 μm). (b) Dendrite angle of the
 4 pTAPP electrodeposited with a scan rate of 2 mV/s at 5 °C. (c) SEM image of the pTAPP dendrite
 5 supported on an amorphous pTAPP, deposited on GC electrode at 2 mV/s and 5 °C. The scale bar in the
 6 inset is 300 nm. (d) The schematic mechanism of dendrite formation during the electropolymerization of
 7 pTAPP. Electropolymerization is carried out in a 5% v/v pyridine in dichloromethane solution containing
 8 0.25 mM TAPP and 0.05 M TEA(PF₆).

9 We evaluate the ORR electrocatalytic performance of the Py-POR-COF films, deposited on GC
 10 electrodes, using a three-electrode electrochemical cell, in an aqueous phosphate buffer solution (PBS).
 11 The experimental procedure is reported in Section 5 of the Supporting Information. Figure 5a presents the
 12 cyclic voltammograms of the prepared films in the electrolyte solutions. For the electrolyte saturated with
 13 oxygen, a salient cathodic peak is observed at ≈ 0.54 V versus reversible hydrogen electrode (RHE). We
 14 attribute this peak to the oxygen electroreduction on the deposited frameworks.

15 We performed rotating disk experiments on the coated electrodes and used the Koutecky-Levich (K-L)
 16 equation to obtain the electron transfer number (n). The estimated values for n were found to be 3.21 ± 0.51
 17 and 3.97 ± 0.44 , for the wire- and dendrite-like samples, respectively. These values suggest that the ORR
 18 is taking place via mixed two- and four-electron pathways (Figure S21).³¹ The larger n for the Py-POR-
 19 COF, compared to the wire-like pTAPP, points to the superior electrocatalytic activity of Py-POR-COF.
 20 Changing the potential scanning rate used for electrodeposition, we observed a change in the onset
 21 potential of the cathodic waves and the normalized ORR current density (Figure S22). As mentioned
 22 earlier, morphology of the electropolymerized Py-POR-COF is also correlated with the scan rate.
 23 Comparing these morphologies (Figure 4a) to the voltammograms in Figure 5b and S22 reveals that the
 24 films with larger crystalline dendrites display higher ORR activity. We expect that such enhanced

1 electrocatalytic activity is correlated with a better crystal quality, i.e., lower density of structural defects
2 and a more ordered arrangement of the Py-POR-COFs, leading to better charge mobility (relative to the
3 amorphous structures).^{17, 32-35} In addition to temperature, scan rate and electrode material, the stabilizing
4 effect of pyridine is yet another factor contributing to the ordered networks of (pyridine-mediated) π - π
5 stacked COFs (Figure S23). For more details on the enhancement of charge mobility and ORR, see Section
6 S5 of the Supporting Information.

7 The pyridine co-crystallization leads to an increased interlayer distance. Hence, in addition to the surface
8 binding sites, the enlarged spacing allows the oxygen species to explore the 3D binding motifs, created
9 by the stacked COF layers. Such motifs (and the resulting confinement) can potentially change the
10 energetics of the ORR intermediates, break some scaling relations and improve the current density.³⁶⁻³⁹
11 Additionally, the stacking pattern, by changing the interlayer vdW and π - π interactions, can change the
12 energetics of different reaction intermediates, and, consequently, the overall catalytic activity. The
13 important role of vdW interactions in tuning the catalytic activity of 2D materials has been previously
14 reported.⁴⁰⁻⁴¹



15
16 **Figure 5.** The electrocatalytic activity of Py-POR-COF in ORR. (a) The cyclic voltammogram of a Py-
17 POR-COF in a phosphate buffer solution (PBS) ($pH=13$) deaerated with argon (Ar) and saturated with
18 oxygen (O_2). The film was deposited at 25 °C and a scan rate of 50 mV/s. (b) The normalized cyclic
19 voltammogram of Py-POR-COF films in an O_2 -saturated PBS with ($pH=13$), presenting a correlation
20 between Py-POR-COF crystallinity and the ORR catalytic performance. The potential scanning rate for
21 ORR was set at 20 mV/s. The scale bars on the SEM image are 60 μm . Here, (i), (ii) and (iii) represent
22 the respective structure of the samples prepared at a deposition temperature of 25 °C.

23 In summary, we reported the in situ electropolymerization of porphyrin derivatives (TAPP) and formation
24 of crystalline domains (Py-POR-COF). We investigated the parameters influencing the
25 electropolymerization of TAPP and developed a methodology to control the growth and deposition of

1 COFs. We demonstrated that the highly-ordered 3D stacking of the Py-POR-COFs enhances the ORR
2 activity of the sample. High crystalline order is achieved by controlling the temperature, potential
3 scanning rate, electrode materials, and through co-crystallization with pyridine. The pyridine sublattice
4 not only stabilizes the Py-POR-COF superlattice, but it also controls the interlayer spacing and stacking
5 in this class of materials.

6 **ASSOCIATED CONTENT**

7 **Supporting Information**

8 The Supporting Information is available free of charge on the ACS Publications website at DOI:

9 General procedures, experimental details of synthesis, electrochemistry studies, and DFT calculations.
10 Characterizations, containing FT-IR, ¹H-NMR spectra, XRD data and crystal structures, SEM images,
11 AFM images, and stability test.

12 **AUTHOR INFORMATION**

13 **Corresponding Author**

14 *snejati2@unl.edu

15 **ORCID**

16 Elham Tavakoli: <http://orcid.org/0000-0002-2077-0577>

17 Arvin Kakekhani: <https://orcid.org/0000-0002-8553-7776>

18 Shayan Kaviani: <http://orcid.org/0000-0002-9868-7757>

19 Mahdi Mohammadi Ghaleni: <http://orcid.org/0000-0002-9824-450X>

20 Mohsen Asle Zaem: <https://orcid.org/0000-0002-5164-6122>

21 Andrew M. Rappe: <https://orcid.org/0000-0003-4620-6496>

22 Siamak Nejati: <http://orcid.org/0000-0002-1807-2796>

23 **Notes**

24 The authors declare no competing financial interest.

25 **ACKNOWLEDGMENT**

26 The research was performed in part in the Nebraska Nanoscale Facility: National Nanotechnology
27 Coordinated Infrastructure and the Nebraska Center for Materials and Nanoscience, which are supported

1 by the National Science Foundation under Award ECCS: 1542182, and the Nebraska Research Initiative.
2 A.K. and A.M.R. acknowledge the support of the US Department of Energy, Office of Basic Energy
3 Sciences, under grant DE-SC0019281. PT acknowledges the scholarship from Chinese Scholarship
4 Council (CSC). We also acknowledge computational support from NERSC of the DOE.

6 REFERENCES

- 8 1. Kandambeth, S.; Dey, K.; Banerjee, R., Covalent Organic Frameworks: Chemistry beyond the
9 Structure. *J. Am. Chem. Soc.* **2019**, *141* (5), 1807-1822.
- 10 2. Lin, G.; Ding, H.; Yuan, D.; Wang, B.; Wang, C., A pyrene-based, fluorescent three-dimensional
11 covalent organic framework. *J. Am. Chem. Soc.* **2016**, *138* (10), 3302-3305.
- 12 3. Day, N. U.; Wamser, C. C.; Walter, M. G., Porphyrin polymers and organic frameworks. *Polym. Int.*
13 **2015**, *64* (7), 833-857.
- 14 4. Chen, X.; Gao, J.; Jiang, D., Designed synthesis of porphyrin-based two-dimensional covalent
15 organic frameworks with highly ordered structures. *Chem. Lett.* **2015**, *44* (9), 1257-1259.
- 16 5. Liu, Q.-Y.; Li, J.-F.; Wang, J.-W., Research of covalent organic frame materials based on porphyrin
17 units. *J. Inclusion Phenom. Macrocyclic Chem.* **2019**, 1-15.
- 18 6. Pachfule, P.; Acharjya, A.; Roeser, J. r. m.; Langenhahn, T.; Schwarze, M.; Schomäcker, R.; Thomas,
19 A.; Schmidt, J., Diacetylene functionalized covalent organic framework (COF) for photocatalytic hydrogen
20 generation. *J. Am. Chem. Soc.* **2018**, *140* (4), 1423-1427.
- 21 7. Huang, N.; Krishna, R.; Jiang, D., Tailor-made pore surface engineering in covalent organic
22 frameworks: systematic functionalization for performance screening. *J. Am. Chem. Soc.* **2015**, *137* (22),
23 7079-7082.
- 24 8. Lin, S.; Diercks, C. S.; Zhang, Y.-B.; Kornienko, N.; Nichols, E. M.; Zhao, Y.; Paris, A. R.; Kim, D.; Yang,
25 P.; Yaghi, O. M., Covalent organic frameworks comprising cobalt porphyrins for catalytic CO₂ reduction
26 in water. *Science* **2015**, *349* (6253), 1208-1213.
- 27 9. Diercks, C. S.; Lin, S.; Kornienko, N.; Kapustin, E. A.; Nichols, E. M.; Zhu, C.; Zhao, Y.; Chang, C. J.;
28 Yaghi, O. M., Reticular electronic tuning of porphyrin active sites in covalent organic frameworks for
29 electrocatalytic carbon dioxide reduction. *J. Am. Chem. Soc.* **2018**, *140* (3), 1116-1122.
- 30 10. Lin, G.; Ding, H.; Chen, R.; Peng, Z.; Wang, B.; Wang, C., 3D porphyrin-based covalent organic
31 frameworks. *J. Am. Chem. Soc.* **2017**, *139* (25), 8705-8709.
- 32 11. Yang, S.; Hu, W.; Zhang, X.; He, P.; Pattengale, B.; Liu, C.; Cendejas, M.; Hermans, I.; Zhang, X.;
33 Zhang, J., 2D Covalent Organic Frameworks as Intrinsic Photocatalysts for Visible Light-Driven CO₂
34 Reduction. *J. Am. Chem. Soc.* **2018**, *140* (44), 14614-14618.
- 35 12. Oldacre, A. N.; Friedman, A. E.; Cook, T. R., A self-assembled cofacial cobalt porphyrin prism for
36 oxygen reduction catalysis. *J. Am. Chem. Soc.* **2017**, *139* (4), 1424-1427.
- 37 13. Peljo, P.; Murtomäki, L.; Kallio, T.; Xu, H.-J.; Meyer, M.; Gros, C. P.; Barbe, J.-M.; Girault, H. H.;
38 Laasonen, K.; Kontturi, K. s., Biomimetic oxygen reduction by cofacial porphyrins at a liquid-liquid
39 interface. *J. Am. Chem. Soc.* **2012**, *134* (13), 5974-5984.
- 40 14. Jahan, M.; Bao, Q.; Loh, K. P., Electrocatalytically active graphene-porphyrin MOF composite for
41 oxygen reduction reaction. *J. Am. Chem. Soc.* **2012**, *134* (15), 6707-6713.
- 42 15. Friedman, A.; Landau, L.; Gonen, S.; Gross, Z.; Elbaz, L., Efficient Bio-Inspired Oxygen Reduction
Electrocatalysis with Electropolymerized Cobalt Corroles. *ACS Catal.* **2018**, *8* (6), 5024-5031.

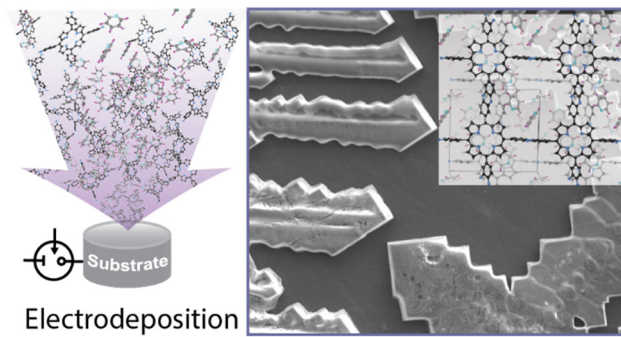
- 1
2 16. Day, N. U.; Wamser, C. C., Poly-tetrakis-5, 10, 15, 20-(4-aminophenyl) porphyrin Films as Two-
3 Electron Oxygen Reduction Photoelectrocatalysts for the Production of H₂O₂. *J. Phys. Chem. C* **2017**, *121*
4 (21), 11076-11082.
- 5 17. Ma, W.; Yu, P.; Ohsaka, T.; Mao, L., An efficient electrocatalyst for oxygen reduction reaction
6 derived from a Co-porphyrin-based covalent organic framework. *Electrochem. Commun.* **2015**, *52*, 53-
7 57.
- 8 18. Zhao, C.-X.; Li, B.-Q.; Liu, J.-N.; Huang, J.-Q.; Zhang, Q., Transition metal coordinated framework
9 porphyrin for electrocatalytic oxygen reduction. *Chin. Chem. Lett.* **2019**, *30* (4), 911-914.
- 10 19. Hisaki, I.; Affendy, N. E.; Tohnai, N., Precise elucidations of stacking manners of hydrogen-bonded
11 two-dimensional organic frameworks composed of X-shaped π -conjugated systems. *CrystEngComm*
12 **2017**, *19* (33), 4892-4898.
- 13 20. Walter, M. G.; Wamser, C. C., Synthesis and characterization of electropolymerized
14 nanostructured aminophenylporphyrin films. *J. Phys. Chem. C* **2010**, *114* (17), 7563-7574.
- 15 21. Hu, Y. Two-dimensional (2D) functional molecular networks. UCL (University College London),
16 2016.
- 17 22. Bidman, T., Oxidation of 2-alkyl-5, 10-dihydrophenazines. *Russ. J. Gen. Chem.* **2004**, *74* (9), 1433-
18 1434.
- 19 23. Hayashi, T.; Hijikata, Y.; Page, A.; Jiang, D.; Irle, S., Theoretical analysis of structural diversity of
20 covalent organic framework: Stacking isomer structures thermodynamics and kinetics. *Chem. Phys. Lett.*
21 **2016**, *664*, 101-107.
- 22 24. Chen, R.; Shi, J. L.; Ma, Y.; Lin, G.; Lang, X.; Wang, C., Designed Synthesis of a 2D Porphyrin-Based
23 sp² Carbon-Conjugated Covalent Organic Framework for Heterogeneous Photocatalysis. *Angew. Chem.,*
24 *Int. Ed.* **2019**, *58* (19), 6430-6434.
- 25 25. Biswal, B. P.; Valligatla, S.; Wang, M.; Banerjee, T.; Saad, N. A.; Mariserla, B. M. K.; Chandrasekhar,
26 N.; Becker, D.; Addicoat, M.; Senkovska, I., Nonlinear Optical Switching in Regioregular Porphyrin
27 Covalent Organic Frameworks. *Angew. Chem.* **2019**, *131* (21), 6970-6974.
- 28 26. Keller, N.; Calik, M.; Sharapa, D.; Soni, H. R.; Zehetmaier, P. M.; Rager, S.; Auras, F.; Jakowetz, A.
29 C.; Görling, A.; Clark, T., Enforcing extended porphyrin J-aggregate stacking in covalent organic
30 frameworks. *J. Am. Chem. Soc.* **2018**, *140* (48), 16544-16552.
- 31 27. Hao, F.; Verma, A.; Mukherjee, P. P., Mesoscale Complexations in Lithium Electrodeposition. *ACS*
32 *Appl. Mater. Interfaces* **2018**, *10* (31), 26320-26327.
- 33 28. Bae, S.; Kim, H.; Lee, H. S., Formation mechanism of PbTe dendritic nanostructures grown by
34 electrodeposition. *Mater. Chem. Phys.* **2017**, *187*, 82-87.
- 35 29. Ding, F.; Xu, W.; Graff, G. L.; Zhang, J.; Sushko, M. L.; Chen, X.; Shao, Y.; Engelhard, M. H.; Nie, Z.;
36 Xiao, J., Dendrite-free lithium deposition via self-healing electrostatic shield mechanism. *J. Am. Chem.*
37 *Soc.* **2013**, *135* (11), 4450-4456.
- 38 30. Popov, K. I.; Nikolić, N. D., General theory of disperse metal electrodeposits formation. In
39 *Electrochemical production of metal powders*, Springer: 2012; pp 1-62.
- 40 31. Kaviani, S.; Mohammadi Ghaleni, M.; Tavakoli, E.; Nejati, S., Electroactive and Conformal Coatings
41 of Oxidative Chemical Vapor Deposition Polymers for Oxygen Electroreduction. *ACS Appl. Polym. Mater.*
42 **2019**, *1* (3), 552-560.
- 43 32. Lin, C. Y.; Zhang, D.; Zhao, Z.; Xia, Z., Covalent organic framework electrocatalysts for clean energy
44 conversion. *Adv. Mater.* **2018**, *30* (5), 1703646.
- 45 33. Kim, T. W.; Jun, S.; Ha, Y.; Yadav, R. K.; Kumar, A.; Yoo, C.-Y.; Oh, I.; Lim, H.-K.; Shin, J. W.; Ryoo, R.,
46 Ultrafast charge transfer coupled with lattice phonons in two-dimensional covalent organic frameworks.
Nat. Commun. **2019**, *10* (1), 1873.

- 1
2 34. Niu, W.; Marcus, K.; Zhou, L.; Li, Z.; Shi, L.; Liang, K.; Yang, Y., Enhancing electron transfer and
3 electrocatalytic activity on crystalline carbon-conjugated g-C₃N₄. *ACS Catal.* **2018**, *8* (3), 1926-1931.
- 4 35. Scholes, D. T.; Yee, P. Y.; Lindemuth, J. R.; Kang, H.; Onorato, J.; Ghosh, R.; Luscombe, C. K.; Spano,
5 F. C.; Tolbert, S. H.; Schwartz, B. J., The Effects of Crystallinity on Charge Transport and the Structure of
6 Sequentially Processed F4TCNQ-Doped Conjugated Polymer Films. *Adv. Funct. Mater.* **2017**, *27* (44),
7 1702654.
- 8 36. Vojvodic, A.; Nørskov, J. K., New design paradigm for heterogeneous catalysts. *Natl. Sci. Rev.* **2015**,
9 *2* (2), 140-143.
- 10 37. Christensen, R.; Hansen, H. A.; Dickens, C. F.; Nørskov, J. K.; Vegge, T., Functional independent
11 scaling relation for ORR/OER catalysts. *J. Phys. Chem. C* **2016**, *120* (43), 24910-24916.
- 12 38. Wan, H.; Østergaard, T. M.; Arnarson, L.; Rossmeisl, J., Climbing the 3D Volcano for the Oxygen
13 Reduction Reaction Using Porphyrin Motifs. *ACS Sustainable Chem. Eng.* **2018**, *7* (1), 611-617.
- 14 39. Szécsényi, Á.; Khramenkova, E.; Chernyshov, I. Y.; Li, G.; Gascon, J.; Pidko, E. A., Breaking Linear
15 Scaling Relationships with Secondary Interactions in Confined Space: A Case Study of Methane Oxidation
16 by Fe/ZSM-5 Zeolite. *ACS Catal.* **2019**, *9* (10), 9276-9284.
- 17 40. Gutzler, R., Band-structure engineering in conjugated 2D polymers. *Phys. Chem. Chem. Phys.*
18 **2016**, *18* (42), 29092-29100.
- 19 41. Tsai, C.; Abild-Pedersen, F.; Nørskov, J. K., Tuning the MoS₂ edge-site activity for hydrogen
20 evolution via support interactions. *Nano Lett.* **2014**, *14* (3), 1381-1387.
- 21

1

"For Table of Contents Only"

2



3

4